Evaluation of Membrane Mimetics for the Native Ion Mobility – Mass Spectrometry Analysis of Membrane Proteins

Iliana Levesque[1‡], Kristine F. Parson[1‡], Sarah M. Fantin[1†], Brandon T. Ruotolo[1*]

[1]Department of Chemistry, University of Michigan, Ann Arbor, MI 48109 USA

ABSTRACT: Membrane protein (MP) structures and functions are intricately linked to their surrounding membrane environments and their respective lipid compositions in addition to influences exerted by unique membrane microdomains (i.e., lipid rafts). Owing to the complexity of their native environments, MPs pose significant challenges to structural biology due to their intrinsic hydrophobic nature rendering them incompatible with aqueous conditions commonly deployed during sample preparation. To overcome these solubility issues, MP studies commonly utilize detergent micelles. In recent years, numerous efforts have been directed toward developing membrane mimetics to facilitate successful solubilization and stabilization of MPs. Collision-induced dissociation (CID) can be employed to remove surrounding molecules from MPs during native mass spectrometry (nMS) experiments, and such methods can be used to evaluate previously inaccessible MPs. However, the differential effects of various membrane mimetics on MP structure and stability remain largely unexplored. In this study, we evaluate a range of MPs, including both transmembrane and monotopic variants, solubilized in detergent micelles, mixed lipid bicelles, and nanodiscs mimetics. Our findings reveal significant differences in collision induced unfolding (CIU) features, stabilities, collision cross-sections (CCS), and RMSD comparisons with values exceeding 26%. These results underscore the importance of considering the choice of membrane mimetics when studying MP structure.

Introduction

Membrane Proteins (MPs) constitute a substantial fraction (~30%) of the human proteome[1] with highly specialized eukaryotic membranes estimated to contain up to 70% MPs.[2-4] Not only does the presence of MPs vary considerably within cell membranes but also they play numerous critical roles across many biological processes including cellular structure, transportation, signaling, and overall cell homeostasis.[5,6] As such, MPs currently represent approximately 30-40% of human drug targets particularly aimed at ion channels, enzymes, and receptors.[7] Despite these crucial roles in human biology, MPs account for only 3% of unique structures in the protein data bank (PDB).[6] This disparity between the significance of MPs and the limited structural information available underscores the ongoing challenges surrounding MP structure determination.

MPs are naturally found either embedded (integral) or on the surface (peripheral) of cellular membranes. At first glance, membranes appear to consist of amphipathic lipids wherein polar head groups and hydrophobic lipid tails associate in a manner to form a hydrophobic lipid-tail core.[8] In reality, membranes exhibit a much greater complexity of highly specialized compositions tailored for specific cellular functions, such as those found in the cytosol, mitochondria, endoplasmic reticulum, Golgi apparatus, and other organelles.[5,8-11] Due to their complex native environments and intrinsic hydrophobicity, the extraction and purification of MPs require the use of solubilization agents and often result in low MP yields and limited long-term stability.[12-14] Consequently, acquiring information to address functional questions regarding MPs has proven challenging and oftentimes hinders ongoing efforts to enhance understanding of diseases and subsequent therapeutic developments. Further, the function and structure of MPs have been shown to be sensitive to the solubilization technique used,[15-17] leading to increased utilization of higher fidelity membrane mimetics. A substantial effort in the last 20 years has been focused on the development and implementation of membrane mimetics capable of more faithfully replicating the cellular environment of MPs, thereby facilitating the study of MPs within a more biologically relevant context.[18]

Native mass spectrometry (nMS) has emerged as a useful technique in the structural biology toolkit, capable of analyzing MPs from various solubilization methods to reveal structural and functional information.[19,20] In nMS workflows, MPs are transferred into the gas phase via nano-electrospray ionization (nESI).[21-22] During this process, MPs remain encapsulated in the membrane mimetic in which they were solubilized until collisional heating causes the surrounding molecules to dissociate from the MP.[23] While much of the work in this field has focused on liberating gas-phase MPs from detergent micelles,[24-32] nMS has successfully detected MPs housed in various membrane mimetics, including amphipols,[33-35] bicelles,[36,37] nanodiscs,[38-42] styrene maleic acid lipid particles (SMALPS),[43,44] and membrane vesicles.[45-49] Overall, nMS used in combination with these membrane mimetics has provided

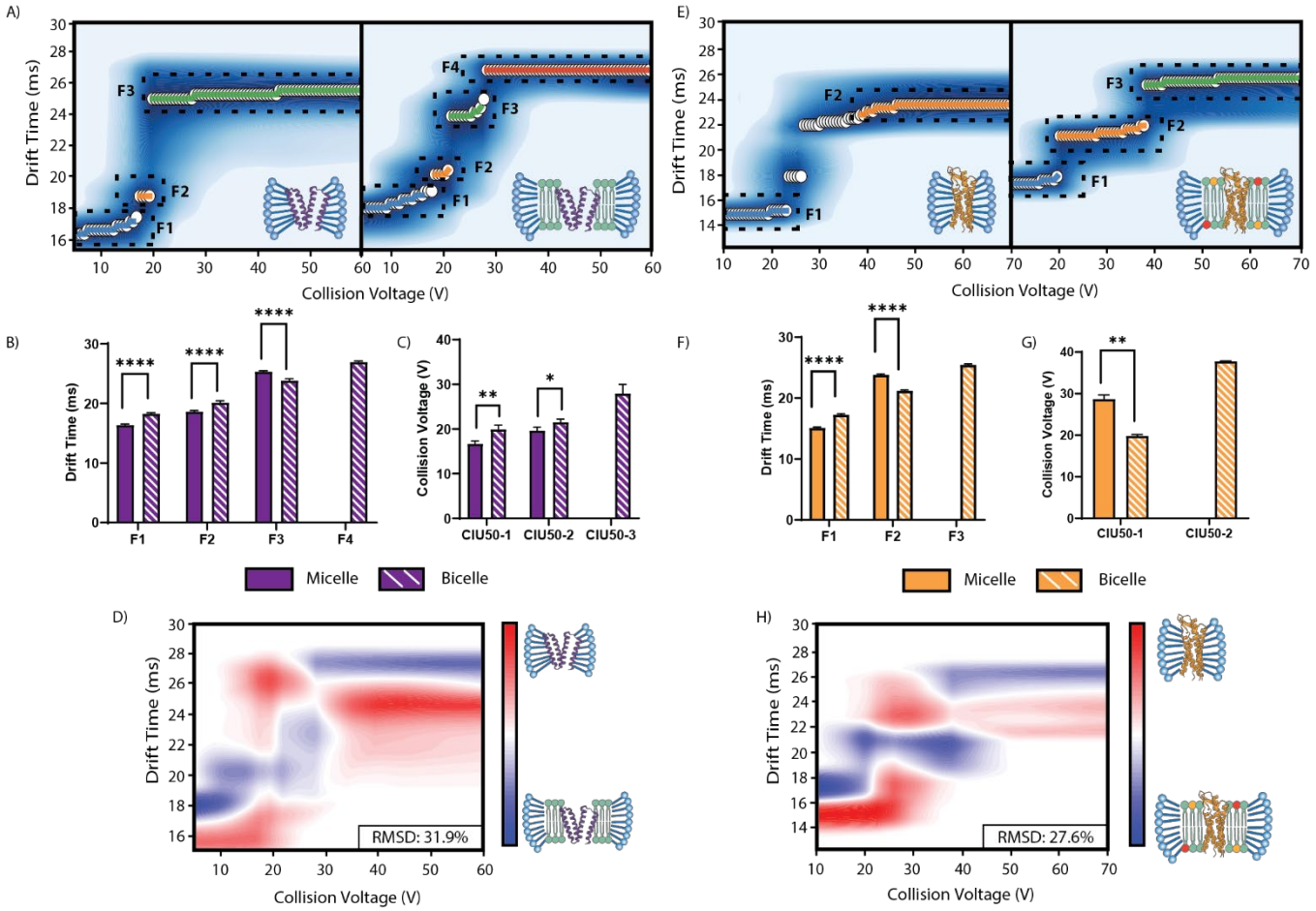

Figure 1. CIU comparisons between GDX 6^+ ions and PMP22 L16P 13^+ ions released from micelles vs bicelles. A) Averaged fingerprints (n=3) of the monomer 6^+ charge state of GDX liberated from DDM detergent micelles show 3 features when liberated from the micelle and 4 features when liberated from the bicelle. B) Feature detection reveals significant differences (**** $p < 0.0001$) between F1-F3. C) CIU50 analysis shows significant differences (** $p < 0.001$) in the CIU 50-1 as well as in the CIU50-2 (* $p < 0.01$) protein stabilities. D) Pairwise RMSD analysis reveals global CIU differences between GDX from a micellar environment vs a bilayer mixed detergent and lipid environment. E) Averaged fingerprints (n=3) of the 13^+ charge state of L16P dimer liberated from C12E8 detergent micelles show 2 features when liberated from the micelle and 3 features when liberated from the bicelle. F) Feature detection reveals significant differences (**** $p < 0.0001$) between F1-F2. G) CIU50 analysis shows significant differences (** $p < 0.001$) in the CIU 50-1 protein stability. H) Pairwise RMSD analysis reveals global CIU differences between L16P 13^+ dimer released from micelles vs. mixed detergent and lipid environment.

direct insights into MP purity,[50] MP oligomeric states,[36,48,51] MP-ligand interactions,[29,31,52,53] stabilities,[31,36,54,55] modifications,[56] and complex formation for both peripheral and transmembrane MPs.[47]

The coupling of ion mobility (IM) separation to nMS (nIM-MS) allows for the measurement of the orientationally averaged size of gas phase MPs,[57] and enables collision-induced unfolding experiments (CIU). In CIU, protein ions are collisionally activated by incrementally increasing an accelerating potential, or collision voltage (CV), resulting in ion heating and subsequent protein ion unfolding. The CIU pathway adopted by protein ions can be tracked through IM separation, and automated workflows for the analysis of CIU fingerprints are supported through widely-available software tools to provide stability and structure information.[58] Although many studies have employed nIM-MS and CIU to reveal structural changes and stabilities of MP complexes,[25, 31, 59-62] CIU analysis of MPs has predominantly focused on those solubilized using a single mimetic, lacking a thorough examination of the consequences of mimetic choice on nIM-MS data, and the information that results from such analyses.

Here, we employ nIM-MS and CIU to systematically investigate MPs reconstituted within multiple categories of solubilization agents, including detergent micelles, bicelles, and nanodiscs (NDs). We employ nIM-MS to assess the ability of CIU to discern the differences in MP structure associated with the solubilization agents used to encapsulate MPs before analysis. We accomplish this by collecting CIU fingerprints for a range of model MP systems solubilized using at least two different methods, such as detergent micelles, sphingomyelin and cholesterol-rich (SCOR) bicelles,[37] POPC-DDMB bicelles, and POPC lipid NDs. Our selection of three model protein systems (the monotopic cytochrome P450 3A4 (CYP3A4), the dimeric L16P variant of the integral peripheral myelin protein

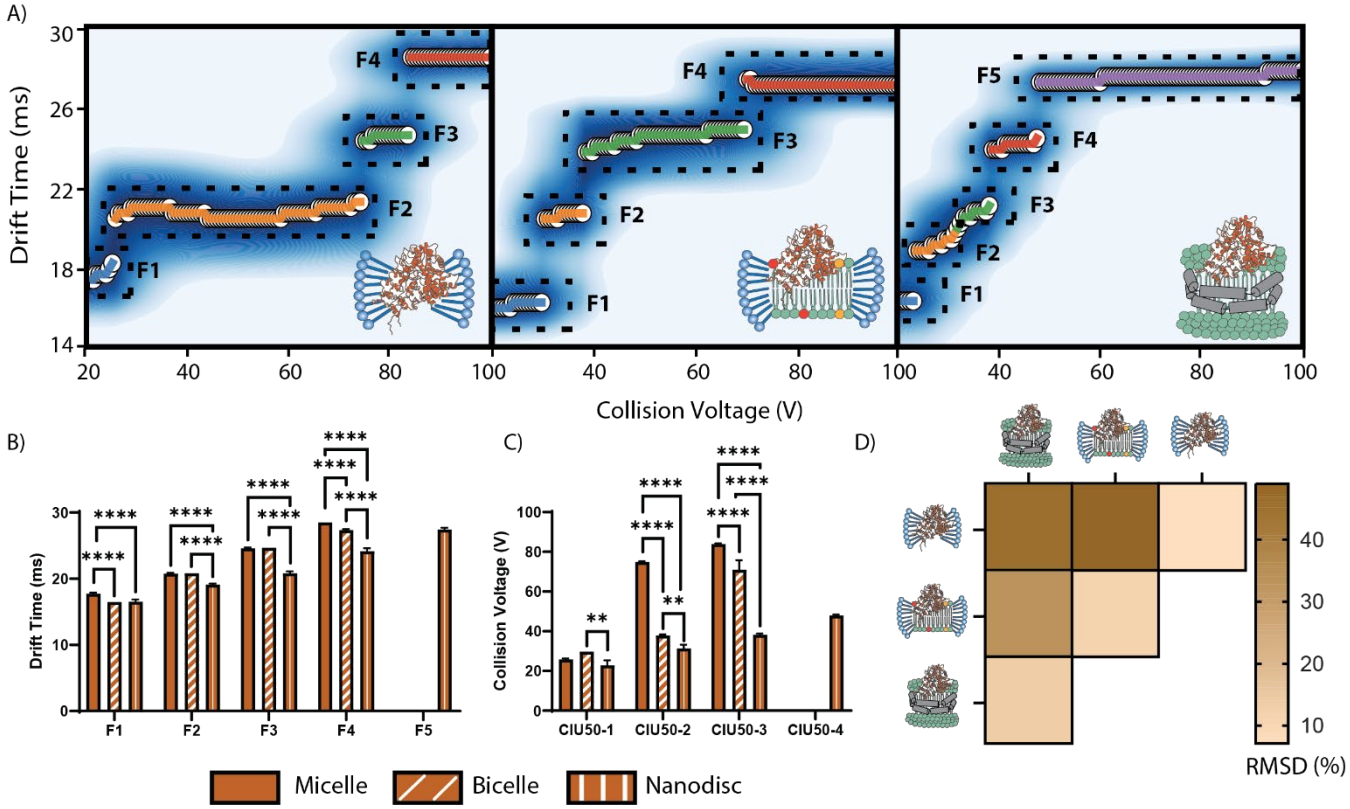

Figure 2. CIU comparisons of CYP3A4 released from OG micelles, SCOR bicelles, and POPC nanodiscs, respectively. A) Averaged fingerprints (n=3) of the monomer 16^+ holo charge state of CYP3A4 liberated from OG detergent micelles and bicelles reveals 4 features while CYP3A4 released from NDs reveals 5 features. B) Feature detection reveals significant differences (**** $p < 0.0001$) between F1-F4. C) CIU50 analysis shows significant differences (**** $p < 0.0001$) in the CIU 50-2 as well as in the CIU50-3 protein stabilities. D) Heat plot of RMSD analysis reveals significant differences between CYP3A4 from a micellar environment vs a bilayer environment.

(PMP22 L16P), wild type PMP22 which contains an 11 kDa soluble tag (PMP22 WT Tagged), and the small multidrug resistance transporter (GDX)) aims to represent a variety of MP structures. Due to the significant and varying levels of chemical noise encountered in our nIM-MS data, we developed a feature-focused denoising strategy that dramatically improves the quality of CIU information obtained for MPs. We find evidence of significant differences across all CIU datasets collected for these MPs as a function of the solubilization agents used in their preparation. These findings underscore the importance of carefully evaluating solubilization agents and their impact on MP structure during nIM-MS workflow development and for MP structural biology campaigns more broadly. We further discuss the broader implications of the local environment on MP structure and stability and address the existing challenges and limitations associated with certain membrane mimetics in conjunction with nIM-MS. Finally, we propose future experiments aimed at elucidating the role of solubilization agents in shaping structural MS data targeting MPs.

Materials and Methods

Membrane Protein Sample Preparation: CYP3A4 was expressed in *E. Coli* and purified using protocols described elsewhere.[63-64] PMP22 WT tagged and the L16P mutant variant were expressed in *E. coli.* using protocols adapted from Schlebach et al.[65] For tagged WT PMP22, the protein did not undergo the final thrombin cleavage step. GDX-Clo (*Clostridiales bacterium* oral taxon 876) was expressed in *E. coli* and purified using protocols previously described.[66] Octaethylene glycol monododecyl ether (C12E8), n-Dodecyl-β-D-Melibioside (DDMB), and n-dodecyl-β-D-maltoside (DDM) were purchased from Anatrace, Octyl β-D-glucopyranoside (OG), membrane scaffold protein 1D1(-), ammonium acetate, sodium chloride, tris(hydroxymethyl)aminomethane (tris), sodium azide, and ethylenediaminetetraacetic acid (EDTA) were purchased from Sigma Aldrich (St. Louis, MO). The lipids 1-palmitoyl-2-oleoyl-glycero-3-phosphocholine [POPC], dimyristoylphosphatidylcholine [DMPC], egg sphingomyelin [eSM] and cholesterol, were purchased from Avanti Polar Lipids (Alabaster, AL). All MPs were screened for appropriate detergent conditions.[67] Samples housed in detergent micelles were simultaneously detergent and buffer exchanged using 10 kDa Amicon Ultra-0.5 centrifugal filter units (MilliporeSigma, Burlington, MA). Starting and ending buffers and detergents conditions before native MS are as follows: 50 µM PMP22 was exchanged from 50 mM Tris, 0.15% DM, 15 mM imidazole, and 1 mM TCEP, and 0.1% DDM, pH 8.0, into 0.02% C12E8 (~4 x CMC), 200 mM ammonium acetate, pH 8.0, 36 µM CYP3A4 was exchanged from 40 mM potassium phosphate, 20% glycerol, pH 7.4 into 40 mM OG, 200 mM ammonium acetate, pH 7.4. 50 µM GDX was exchanged from 100 mM NaCl, 10 mM HEPES, pH 8.0 buffer with 4 mM DM, into 0.3 mM DDM, 200 mM Ammonium acetate, pH 8.0. Samples housed in SCOR bicelles were prepared as described in the supplemental methods of Fantin et al.[36] and were then buffer exchanged using 10 kDa Amicon Ultra-0.5 centrifugal filter

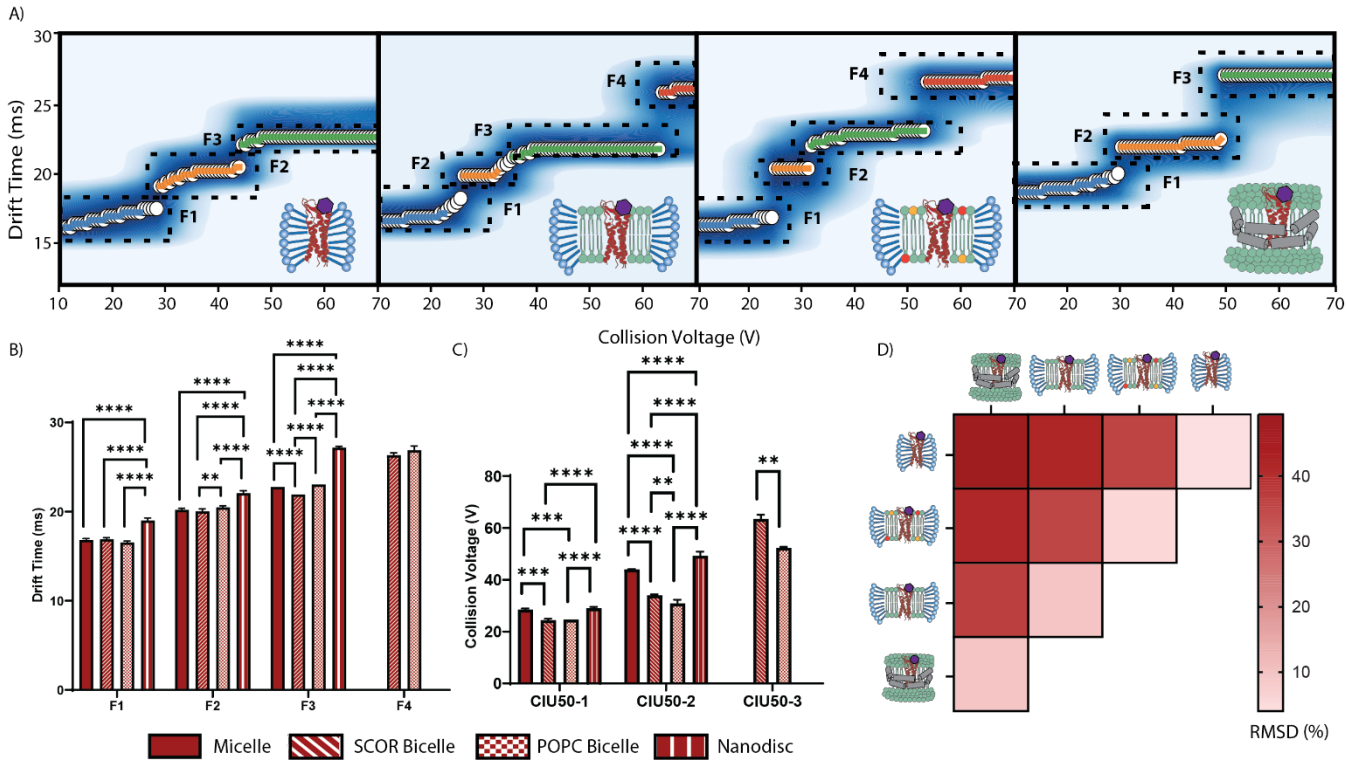

Figure 3. PMP22 WT with a soluble tag released from C12E8 micelles, SCOR bicelles, POPC-DDMB bicelles, and POPC nanodiscs, respectively. A) Averaged fingerprints (n=3) of the 9+ charge state of PMP22 WT Tagged liberated from C12E8 detergent micelles, SCOR bicelles, POPC-DDMB bicelles, and POPC nanodiscs show 3 features when liberated from the micelle and nanodisc, and 4 features when released from the bicelle environments. B) Feature detection reveals significant differences (**** $p < 0.0001$) between F1 and F3, and (**** $p < 0.0001$ and ** $p < 0.01$ in F2. C) CIU50 analysis shows significant differences (**** $p < 0.0001$ and *** $p < 0.0001$) in the CIU 50-1 as well as in the CIU50-2 protein stabilities. D) Heat plot of RMSD analysis reveals significant differences between PMP22 WT from a micellar environment vs bilayer environment.

units. Bicelle samples were not detergent exchanged and the DDMB concentration was held at 1 x CMC to preserve the bicelles q ratio (0.33) Specifically, 40 µM PMP22 WT, PMP22 L16P or GDX in 10 mM acetate buffer (pH 5.0) containing 100 mM NaCl, 0.2% SCOR bicelle or (PMP22-wt only) 0.2% POPC bicelles (q = 0.33), 1 mM EDTA, 5 mM TCEP, and 0.3 mM DDMB was exchanged into 200 mM ammonium acetate, 0.3 mM DDMB, pH 8.0 using 10 kDa Amicon Ultra-0.5 centrifugal filter units. PMP22 WT and GDX were incorporated in MSP1D1 NDs and CYP3A4 were incorporated into MSPE3D1 NDs as described by the Sligar lab[68,69] with the final purification SEC step buffer exchanging into 200 mM Ammonium acetate.

Native IM-MS and CIU Experiments: All nIM-MS and CIU data were collected using a Synapt G2 HDMS IM-Q-ToF mass spectrometer (Waters, Milford, MA), with a direct infusion nESI source set to positive ion mode. Instrument settings were tuned for each protein system and mimetic to generate intact protein ions while completely dissociating detergents, lipids, and scaffold protein before the IM separator, including appropriately tuned settings for the source temperature (30-40 °C), source gas flow (50 mL/min), and the sampling cone (120 V). The traveling wave height and wave velocities in the trap, IM, and transfer region, as well as the helium cell flow rate, were identical for each protein system across mimetics. For PMP, GDX and CYP, trapping cell wave velocity and height were 115 m/s and 0.1 V, IMS wave velocity and height were 250 m/s and 15 V, transfer cell wave velocity and height were 300 m/s and 10 V. An accelerating potential of 70 V in the transfer region was used to dissociate empty solubilization agents for all systems except CYP in NDs, which only required 10 V. All CIU analyses were performed by increasing the trap collision voltage at 5 V increments across ranges tuned for each system. All data collection was performed in triplicate.

Data Processing and Statistical Analysis: nIM-MS data were analyzed in DriftScope and Masslynx V4.1 software (Waters, Milford, MA). CIU data from selected charge states were extracted into a text-based format using TWIMExtract,[70] then processed and analyzed using CIUSuite 2.3.[58,71] Data processing included two or three rounds of 2D Savitzky-Golay smoothing with a window of five bins and interpolation of the collision voltage axis by a factor of four. $^{TW}CCS_{He}$ experimental collision cross-section conversions were performed using IMSCal software and carry an error of ~2-3%.[72] Where possible, theoretical CCSs were calculated from crystal structures[73] and homology models[74,75] using IMPACT.[72,76] In the case of PMP22 L16P dimers, no structural data on PMP22 oligomers has been previously reported. PMP22 L16P experimental CCS values were applied as restraints in computational docking experiments[89] to generate a dimer homology model from the PMP22 monomer homology model structure.[74] The resultant simulations generated 10,000 structures with corresponding Rosetta Scores, and theoretical CCS values were calculated for the highest-scoring structures.

The data were recorded and graphed using GraphPad Prism 10.2.1. The statistical analysis was conducted using 2-way or 3-way ANOVA tests, with statistical significance indicated by a p-value <0.05. Šidák multiple comparison corrections were applied where applicable. Feature-focused denoising (FFD) is

employed to address significant chemical noise present in all CIU data resulting from membrane mimetics. This chemical noise, attributed to excess detergent or lipid molecules, particularly affects regions of lower and higher drift times ranging from 5-100 V. Each solubilization method yields distinct signal-to-noise (S/N) profiles, with variations in background noise across CIU fingerprints obscuring certain features and hindering CIU50 stability analysis. Consequently, low confidence in root-mean-square deviations (RMSD) analyses arises due to the difficulty in distinguishing CIU features associated with MPs. To ensure unbiased analysis, noise is first removed from the text-based TWIM files before analysis in CIUSuite 2.3, enabling robust cross-comparisons of MP CIU data obtained across diverse mimetics.

Feature Focused Denoising: The FFD workflow employs user-defined rectangular masks to selectively preserve identified CIU features during preliminary feature detection analysis. Subsequently, these masks are applied to reprocess the data, focusing on retaining apex values of arrival time distributions at each collision voltage under standard feature detection mode. The rectangular masks enclose points for the feature-length within an allowed width correlated to feature intensities, effectively eliminating noise from non-protein areas while emphasizing and prioritizing protein features without compromising signal intensity. We validated this novel denoising workflow by comparing CIU analysis before and after noise removal (Figure S7). The results showed no significant differences in reported features and CIU50 values. Additionally, confidence in feature detection and CIU50 measurements doubled with the associated reduction in standard deviation values.

Results and Discussion

Comparing CIU of Transmembrane Protein Complexes Liberated from Detergent Micelles and Bicelles. We began our CIU-MP-mimetic screening with the small multidrug resistance (SMR) transporter protein GDX, which has previously been crystallized bound to a monobody.[73] SMRs are distinguished by their unique dual-topology antiparallel dimers. Among the more extensively studied SMRs is EmrE; past reports have identified EmrE in monomer-dimer equilibria and have demonstrated the influence of the membrane environment on dimerization.[77] To our knowledge, GDX-CLO has not been studied previously using nIM-MS. The nIM-MS spectra of GDX yield multiple ion populations corresponding to the monomer and dimer forms upon liberation from DDM micelles (Figure S1 A) and exclusively monomers upon liberation from POPC-DDMB bicelles (Figure S1 B). When liberated from DDM micelles, a charge state distribution (CSD) between 4^+ to 10^+ corresponded to the monomer, while a CSD of 8^+ to 11^+ corresponded to the dimer. Conversely, For GDX liberated from POPC-DDMB bicelles, signals for lower charge states of monomer between 4^+ to 8^+ predominate. We selected GDX 6^+ monomer ions for CIU analysis due to their intensity and minimal overlap with chemical noise signals. Interestingly, CIU data collected for 6^+ GDX monomers in the micelle environment exhibit three features (16.37 ± 0.13, 18.61 ± 0.17, and 25.32 ± 0.13 ms, respectively), while CIU data extracted from the same ions, but released from bicelles, exhibit four features (18.30 ± 0.13, 20.12 ± 0.26, 23.86 ± 0.22, and 26.97 ± 0.13 ms, respectively) (Figure 1A, B). These findings illustrate that GDX adopts distinct conformations and oligomeric states when released from differently constructed membrane mimetic environments.

To further quantify the global structural differences in the CIU fingerprints of GDX from micelles vs. bicelles, RMSD analyses were conducted (Figure 1D). The RMSD values obtained indicate a significant difference in the higher-order structures (HOS) GDX monomers. The RMSD value of 31.9% generated in this comparison is 3.6-6.8 times the baseline of the micelle and bicelle replicates (4.7 ± 0.7% and 8.9 ± 3.8%, respectively). Shifting our focus to assessing differences in CIU50 stabilities between GDX liberated from DDM micelles vs POPC-DDMB bicelles, CIU50 analyses reveal that GDX from DDM micelles undergoes complete unfolding at lower collision voltages compared to GDX from the bicelle environment. Specifically, CIU50-1 values corresponding to the first transition are recorded at 16.67 ± 0.54 V for the micelle and 19.97 ± 0.73 V for the bicelle environment. Similarly, CIU50-2 values confirm the destabilizing effects of the micelles on GDX monomer ions, resulting in 19.63 ± 0.62 V compared to 21.57 ± 0.53 V from the bicelle environment (Figure 1C). Interestingly, similar bicelle-related stabilizing effects have been reported for another SMR MP, EmrE.[77]

Conversion of IM drift times to CCS values also highlights conformational differences (Figure S6 A) across our GDX samples. A CCS analysis of 6^+ GDX monomers indicates that GDX liberated from POPC-DDMB bicelles has a CCS of 1404 Å^2, whereas the same ions prepared in DDM micelles have a CCS value of 1350 Å^2. Notably, when compared to the theoretical CCS value (1476 Å^2) calculated from the crystal structure (6WK8) of monomer GDX,[73] which was modified to convert the dimer into a monomer utilizing CHARMM-GUI[78] and remove the bound monobody and small molecule ligands. While our analysis does not include a molecular dynamics step to compact our GDX monomer model, we note that CCS measurements recorded for GDX released from the bicelle environment are closer to the uncompressed GDX monomer model than those CCS values observed for GDX ions liberated from other membrane mimetics. This result suggests that the bicelle environment may induce a more native-like conformation that is more stabilizing to GDX.

Next, we shifted our focus to a transmembrane MP solubilized in micelles and bicelles. For these experiments, we utilized PMP22, a protein involved in the myelination of neurons. Previous studies have reported that PMP22 L16P, a pathogenic mutant associated with Charcot-Marie-Tooth disease, forms a greater amount of dimer when solubilized in bicelles compared to micelles.[36] Here, we evaluated differences in the CIU data recorded for PMP22 L16P when released from different membrane environments to further evaluate the role of detergent bicelles and micelles in stabilizing various MP structures. The nIM-MS spectra recorded for L16P released from micelles and bicelles are shown in Figure S1 C, D. When released from C12E8 micelles, monomer and dimer signals are observed. We detect monomer ion populations with a CSD between 6^+ to 10^+ and a dimer ion population with a CSD between 10^+ to 15^+. PMP22 L16P released from SCOR bicelles results in a monomer CSD between 5^+ to 10^+, and a dimer CSD between 10^+ to 15^+. We elected to perform CIU analysis on 13^+ dimeric L16P PMP22 ions due to the intensity and minimal noise overlap of the signals detected (Figure S1 C, D).

The CIU data presented in Figure 1E for PMP22 L16P dimer 13^+ ions reveals distinct features and CIU50 transitions for samples prepared in micelles and bicelles. PMP22 L16P dimer released from C12E8 micelles reveals two features (15.10, ± 0.13 and 23.81 ± 0.13 ms, respectively), while the MPs released from the SCOR bicelle environment reveals three features (17.26 ± 0.13, 21.17 ± 0.13, and 25.44 ± 0.13 ms, respectively; Figure 1F). In contrast to our GDX dataset, a comparison of CIU50 values indicates that L16P PMP22 dimers released from micelles are stabilized when compared to their bicelle-encapsulated analogs, with CIU50-1 shifting from 28.67 ± 0.82 V from

the micelle to 19.83 ± 0.26 V in the bicelle (Figure 1G). Additionally, RMSD comparisons of the averaged micelle and bicelle replicates result in a 27.6% difference (Figure 1H), over twice the average RMSD baseline of the micelle (12.6 ± 4.3%) and the bicelle (3.8 ± 0.5%).

A CCS analysis of the 13^+ dimer liberated from C12E8 micelles resulted in a CCS value of 2953 Å^2, while the same ion liberated from the bicelle environment resulted in a CCS value of 2654 Å^2 (Figure S6 B). Similarly to GDX, the CCS values recorded for PMP22 L16P ions released from bicelles more closely agreed with the theoretical CCS estimates (2615 Å^2) From these CCS analyses, we can conclude that L16P released from the C12E8 micelles environment is more compact in structure when compared to PMP22 L16P released from bicelles. In contrast to the GDX data discussed above, PMP22 L16P dimers appear stabilized in micelle rather than bicelle environments, despite their greater abundance in the presence of the latter mimetic. However, taken together, our CCS and CIU data indicate that bicelle and micelle environments promote significantly different structures in transmembrane MPs, underscoring the importance of the selected membrane mimetic on transmembrane MP structure.

Tracking the Influence of Membrane Mimetics on a Monotopic Membrane Protein. While previous nMS reports have primarily focused on multi-pass integral MPs, recent endeavors have extended these techniques to monotopic proteins.[79] Monotopic proteins possess large aqueous domains in addition to regions that interact with but do not traverse, the lipid bilayer. This dual nature often complicates their biophysical characterization.[80] Consequently, single-pass and monotopic MPs, which are embedded in the membrane with a single alpha helix, are often investigated in truncated forms that exclude the membrane-associated components.[80] However, to study the role of the membrane on the structure and function of such MPs, mimetics are needed to replicate the lipid bilayer found in cellular membranes, thereby preserving the overall structure of monotopic MPs. CYP3A4 has been previously studied in NDs, with multiple incorporation protocols published.[16,81]

The CYP family of proteins comprises enzymes crucial for drug metabolism.[64] They exhibit binding affinity for a diverse range of drugs and have previously been observed to also bind detergent molecules.[82] Therefore, we conducted a thorough detergent screen[67] to identify detergent conditions that prevent the formation of CYP-detergent complexes. This screen led to the selection of OG for subsequent nIM-MS analyses. The nIM-MS spectra of CYP3A4 liberated from OG micelles, SCOR bicelles, and CYP3A4 in POPC NDs are shown in Figure S2 A-C. CYP3A4 released from OG detergent micelles exhibits a CSD that includes 13^+ to 17^+ ions. While the MS signals appear broad relative to soluble systems of comparable size,[83] no distinct detergent binding is observed. Deconvolution of these peaks produces an intact mass that corresponds to CYP3A4 plus its heme cofactor, indicating the detection of the holo protein state under these conditions (Table S1). Upon release from SCOR bicelles, a CSD including 14^+ to 18^+ ions is observed, with the holo, heme-bound, and POPC lipid-bound states discernable. Finally, the liberation of CYP3A4 from POPC NDs, assembled using the MSP3ED1 scaffold protein via a microfluidic device,[63] yields a CSD including 13^+ to 17^+ ions. Signals associated with CP3A4 released from NDs exhibit significantly enhanced mass resolution compared to the detergent conditions, enabling the identification of apo, holo CYP3A4, and POPC lipid-bound states. All three nIM-MS datasets reveal monomodal and short IM drift times indicative of native-like CYP ions.

The CYP3A4 holo 16^+ ion was chosen to further explore the impact of membrane mimetics on CYP structure under these conditions. Following CIU experiments of the 16^+ ions (Figure 2A), the CIU data reveals four features from CYP3A4 ions released from both the micelle and bicelle environments, while five features are observed from ions ejected from NDs. When CYP3A4 is released from OG micelles, we observe CIU features at 17.74 ± 0.13, 20.75 ± 0.13, 24.60 ± 0.13, and 28.52 ms, respectively (Figure 2B). When released from the bicelle environment, we see all four features within a 1.3 ms drift time variance when compared to CYP3A4 ions released from micelles (16.46, 20.84, 24.68, and 27.34 ± 0.13 ms, respectively). Examining CYP3A4 released from NDs, similar features are observed with the addition of an additional feature (16.55 ± 0.26, 19.11 ± 0.13, 20.84 ± 0.22, 24.14 ± 0.40, and 27.43 ± 0.22 ms, respectively) (Figure 2B). Although there are minimal differences in the CIU features we record for CYP3A4 across all three mimetic conditions, significant differences are observed in the CIU50 values observed for CYP3A4 ions released from each mimetic. For example, CYP3A4 from OG micelles exhibits CIU50 values of 25.83 ± 0.39, 74.87 ± 0.31, and 83.83 ± 0.31 V, while CYP3A4 released from SCOR bicelles produces CIU50 values of 29.70, 37.83 ± 0.41, and 70.93 ± 4.00 V, respectively. Meanwhile, CYP3A4 liberated from the POPC NDs exhibits CIU50s of 23.0 ± 2.00, 31.27 ± 1.61, 38.20 ± 0.57, and 47.83 ± 0.50 V (Figure 2C). These results highlight the extent of the differences in CYP3A4 structure when liberated from micelles, bicelles and NDs, despite retaining similar CIU features across the data collected here.

Further, RMSD analyses reveal significant wholistic differences across our CYP3A4 CIU data, with the largest differences observed between ions released from OG micelles and those produced from SCOR bicelles (49.0%), followed by comparisons between CYP3A4 ions released from the micelle and nanodisc environments (45.6%) (Figure S3). Remarkably, the lowest RMSD value we observe, 28.6%, is observed between the ND and SCOR bicelle environments, both of which contain POPC lipids in their bilayer constructs (Figure 2D). All RMSD values are at least two times greater than all the baseline values recorded for technical replicates (RMSDs between 7.1-13.8% across all four mimetics, Figure S5). Variations in adduction levels across the MS data recorded for ions generated under these conditions (Figure S2) are also noted, with prior reports indicating that such differences in adduct populations can impact CIU data.[84] Finally, modest differences are detected in holo CYP 16^+ CCS values, with CYP3A4 released from OG micelles resulting in 3451 Å^2 and those from NDs having a value of 3318 Å^2. Our predicted CCS for CYP is 3383 Å^2, indicating that both conditions produced CYP ions within 3% of predictions produced from X-ray data, with NDs producing a more compact state (Figure S6 C).

CIU Data Indicates Structural Changes in PMP22 Liberated from Micelles, Bicelles, and Nanodiscs. After observing the differences between GDX and PMP22 L16P liberated from micelles and bicelles, our next objective was to compare additional mimetics and further broaden our survey of transmembrane MPs. To achieve this, we introduced POPC-DDMB bicelles into our comparative workflows. We opted to continue studying monomeric protein ions to facilitate comparisons across all three solubilization techniques and circumvent challenges encountered in generating sufficient signal intensities for CIU. Hence, we selected a version of PMP22 WT incorporating an 11 kDa soluble tag, referred to as WT-Tagged PMP22, for our investigations. The inclusion of this tag rendered WT-Tagged PMP22 more amenable to ND sample preparation for nMS.

Specifically, the penta-histidine tag included in the sequence enabled us to utilize a nickel affinity resin to purify the ND-associated protein. It is noteworthy that, for this purpose, the his tag-free construct of MSP1D1(-) was employed in these experiments.

WT-Tagged PMP22 can be effectively liberated and detected from C12E8 micelles, SCOR bicelles, POPC-DDMB bicelles, and POPC MSP1D1(-) NDs. Signals corresponding to 7^+ to 15^+ ions of monomeric WT Tagged PMP22 were observed when the protein was solubilized in micelles and bicelles (Figure S4 A-C). However, when WT Tagged PMP22 was housed within NDs, nIM-MS data indicated significant overlap with MSP1D1(-) signals, resulting in reduced observable charge states to 7^+ to 12^+ (Figure S4 D). Ultimately, after careful analysis, we determined that the 9^+ charge state of PMP22 WT Tagged was the most suitable for CIU analysis due to its minimal overlap with MSP1D1(-) signals produced from our ND samples.

CIU fingerprints produced from PMP22 WT Tagged 9^+ ions released from C12E8 micelles and SCOR bicelles exhibited three similar features at approximately 17.0 ms, 20.0 ms, and 22.0 ms (Figure 3A). However, akin to observations with GDX and PMP22 L16P as discussed earlier, an additional feature at 26 ms was observed from PMP22 WT-Tagged ions when liberated from the bicelle environments. Upon liberation from the ND environment, PMP22 WT-Tagged revealed three features at 19.0 ± 0.25, 22.10 ± 0.22, and 27.20 ± 0.13 ms. Notably, this time, feature detection analysis indicates that the micelle and nanodisc environments induce the most distinct structural conformations in PMP22 WT-Tagged, with all three transitions observed at higher drift times, indicative of a more unfolded conformation upon liberation from the ND (Figure 3B).

This information, when combined with the CIU50-1 and CIU50-2 values recorded during our experiments, further highlights the structural differences in MP structure induced between the mimetics probed in our survey (Figure 3C). For WT-Tagged PMP22 liberated from micelles, we record CIU50-1 at 28.47 ± 0.39 V and CIU50-2 at 44.0 ± 0.08 V. In contrast, when released from the NDs, we observe CIU50-1 and CIU50-2 values of 29.00 ± 0.42 V and 49.27 ± 1.30 V, respectively. The CIU50-1, CIU50-2 and CIU50-3 values recorded for PMP22 ions released from SCOR bicelles are observed to be 24.40 ± 0.45, 33.97 ± 0.34, and 63.43 ± 1.30 V, respectively. Conversely, when PMP22 WT-Tagged is released from POPC-DDMB bicelles, CIU50-1-3 values correspond to 24.60 ± 0, 30.87 ± 1.18, and 52.33 ± 0.26 V (Figure 3B). Collectively, these results suggest that WT Tagged PMP22 ions liberated from NDs adopt the most stabilized conformation from all of the mimetics screened here, whilst the bicelles are the most destabilizing in this case.

To further investigate mimetic-dependent changes in CIU fingerprints collected for the monomeric WT Tagged PMP22 9^+ ions, a comprehensive RMSD analysis was conducted across all four CIU datasets as shown in Figure 3D. Notably, WT-Tagged PMP22 ions released from the SCOR bicelles and POPC-DDMB bicelles exhibited the lowest RMSD difference in our analysis at 35.0%, indicating relatively similar PMP22 structures. Conversely, the micelle and ND environments resulted in the highest global differences, with an RMSD difference of 49.4%, approximately two times greater than the ND baseline for replicate analysis (RMSDs between 4.0-9.7% in all four mimetics) (Figure S5).

A CCS analysis of WT-Tagged PMP22 9^+ ions produced from samples containing all the mimetics discussed above was found to yield similar values. Specifically, the recorded CCS values for WT Tagged PMP22 were as follows: micelles: 1932 $Å^2$, SCOR bicelles: 1918 $Å^2$, POPC-DDMB bicelles: 1905 $Å^2$, and POPC NDs: 1996 $Å^2$ (Figure S6 D). While we observe that WT-Tagged PMP22 released from POPC-DDMB bicelles have the most compact CCS values, there is no available high-resolution structure for the WT-Tagged PMP22 construct to which we can accurately compare our CCS values to assess their proximity to its native fold. However, CIU data indicate that WT-Tagged PMP22 adopts different conformations within these differently constructed POPC bilayers. Additionally, detergents may play a role in orienting lipids to form a bilayer differently than MSP, thereby causing PMP22 to adopt different conformations.

Conclusions

MS methods have been extended to directly analyze MPs solubilized using various techniques, and our study demonstrates how nIM-MS and CIU methods can be deployed to evaluate the structural consequences of storing MPs in low fidelity membrane mimetics such as detergent micelles or higher fidelity membrane mimetics such as mixed lipid bicelles and NDs. Additionally, the development of FFD greatly enhanced our ability to make quantitative RMSD comparisons between various MPs released from different mimetics. Our CIU and CCS dataset covers four different MPs solubilized in detergent micelles, SCOR bicelles, POPC-DDMB bicelles, and NDs. We observe minimal differences in low energy CCS values of all the MPs studied herein, but significantly different CIU fingerprints, highlighting the ability of nIM-MS to detect subtle structural differences based on MP environments alone. In the case of CYP3A4, we observe excess detergent, salt, and glycerol adduction, potentially leading to increased stability as observed by CIU for CYP3A4 samples analyzed from micelle samples relative to ND samples. Similarly, our results suggest that SCOR bicelles may support more compact gas-phase structures than C12E8 micelles for PMP22 L16P dimers. Additionally, GDX produces significantly different CIU data when liberated from environments containing detergent compared to ions liberated from a lipid-based environment. Indeed, these data suggest not only compaction of the MP but also stabilization. Further, CIU fingerprints collected across four different mimetics for WT Tagged PMP22 ions exhibit differences primarily attributed to variations in PMP22 conformation promoted in each membrane mimetic.

Overall, extensive CIU and nIM-MS evidence suggests that MP structure strongly depends on the solubilization method used to house the protein prior to liberation in the gas phase. Our data also reveal that solubilization techniques can significantly influence the robustness of the nIM-MS data collected. However, from our data, we cannot determine whether the differences are a function of the lipid composition (SCOR mixed lipids versus POPC) or the solubilization methods used (monolayer versus bilayer). Despite the ongoing analytical challenges associated with the utilization of membrane mimetics necessitating dissociation for the isolation of MPs, advancements in ionization and activation techniques,[56,85,86] alongside the development of detergents engineered to be more compatible with nMS,[87,88] offer promising prospects for the field. To further advance the analysis of MP structure using nIM-MS and CIU, studies should aim to dissect the biophysical contributions of lipid composition and mimetic structures to the observed differences in MP structure and stability. Additionally, there is still a need for an empirical characterization of best practice MP-mimetic sample preparation methods for downstream nIM-MS analysis that explore optimized detergent: MP or lipid: MP ratios. Finally, extending this research to a broader array of protein systems, such as GPCRs, could be crucial for defining the

role of nIM-MS in assessing solubilization agents for applications like MP cryo-EM or pharmaceutical screens.

ASSOCIATED CONTENT

Supporting Information. The Supporting Information is available free of charge on the ACS Publications website.

Additional ion mobility mass spectra, peak identifications, CIU RMSD plots, collision cross sections, and protein mass analysis tables (file type, i.e., PDF)

AUTHOR INFORMATION

Corresponding Author

* Brandon T. Ruotolo – Department of Chemistry, University of Michigan, Ann Arbor, MI 48109, United States; Phone: +1 (734) 615-0198; email: bruotolo@umich.edu; Fax: +1 (734) 615-3718.

Authors

‡**Iliana Levesque** – *Department of Chemistry, University of Michigan, Ann Arbor, Michigan 48109, United States*

‡**Kristine F. Parson** – *Department of Chemistry, University of Michigan 48109, United States*

Present Address: Fujifilm Diosynth Biotechnologies, Morrisville, North Carolina 27560, United States

†**Sarah M. Fantin** – *Department of Chemistry, University of Michigan, Ann Arbor, Michigan 48109, United States*

Present Address: Hanover College, Hanover, Indiana 47243, United States

Author Contributions

‡These authors contributed equally to this work.

Notes

The authors declare that they have no competing financial interest regarding this work.

ACKNOWLEDGMENT

The authors would like to acknowledge the laboratories of Charles Sanders at Vanderbilt University, Melani Ohi at the University of Michigan, and Randy Stockbridge at the University of Michigan for providing protein samples. The authors would also like to thank Anna Anders and Michael Armbruster, members of the Ruotolo research group for their helpful discussions and feedback on this manuscript. Membrane protein research in the Ruotolo Lab is supported by the National Institute of Health under Grants GM105942.

REFERENCES

1. Aguayo-Ortiz R.; Creech J.; Jiménez-Vázquez E. N.; Guerrero-Serna G.; Wang N.; da Rocha A. M.; Herron T.J.; Espinoza-Fonseca L. M. A Multiscale approach for Bridging the Gap between Potency, Efficacy, and Safety of Small Molecules Directed at Membrane Proteins. *Sci Rep* **2021**, 11, 16580. https://doi.org/10.1038/s41598-021-96217-7
2. Wallin, E.; Heijne, G. V. Genome-Wide Analysis of Integral Membrane Proteins from Eubacterial, Archaean, and Eukaryotic Organisms: Membrane Protein Topology. *Protein Science* **1998**, 7 (4), 1029–1038. https://doi.org/10.1002/pro.5560070420
3. Shimizu, K.; Cao, W.; Saad, G.; Shoji, M.; Terada, T. Comparative Analysis of Membrane Protein Structure Databases. *Biochimica et Biophysica Acta (BBA) - Biomembranes* **2018**, 1860 (5), 1077–1091. https://doi.org/10.1016/j.bbamem.2018.01.005
4. Moraes, I.; Evans, G.; Sanchez-Weatherby, J.; Newstead, S.; Stewart, P. D. S. Membrane Protein Structure Determination — The next Generation. *Biochimica et Biophysica Acta (BBA) - Biomembranes* **2014**, 1838 (1), 78–87. https://doi.org/10.1016/j.bbamem.2013.07.010
5. Almén, M. S.; Nordström, K. J.; Fredriksson, R.; Schiöth, H. B. Mapping the Human Membrane Proteome: A Majority of the Human Membrane Proteins Can Be Classified According to Function and Evolutionary Origin. *BMC Biol* **2009**, 7 (1), 50. https://doi.org/10.1186/1741-7007-7-50
6. Deamer, D. Membranes and the Origin of Life: A Century of Conjecture. *J Mol Evol* **2016**, 83 (5–6), 159–168. https://doi.org/10.1007/s00239-016-9770-8
7. Tan, S.; Tan, H. T.; Chung, M. C. M. Membrane Proteins and Membrane Proteomics. *Proteomics* **2008**, 8 (19), 3924–3932. https://doi.org/10.1002/pmic.200800597
8. Membrane Biophysics; Wang, H., Li, G., Eds.; Springer Singapore: Singapore, **2018**. https://doi.org/10.1007/978-981-10-6823-2
9. Cullis, P. R.; De Kruijff, B. Lipid Polymorphism and the Functional Roles of Lipids in Biological Membranes. *Biochimica et Biophysica Acta (BBA) - Reviews on Biomembranes* **1979**, 559 (4), 399–420. https://doi.org/10.1016/0304-4157(79)90012-1
10. Cho, W.; Stahelin, R. V. Membrane-Protein Interactions in Cell Signaling and Membrane Trafficking. *Annu. Rev. Biophys. Biomol. Struct.* **2005**, 34 (1), 119–151. https://doi.org/10.1146/annurev.biophys.33.110502.133337
11. Phillips, R.; Ursell, T.; Wiggins, P.; Sens, P. Emerging Roles for Lipids in Shaping Membrane-Protein Function. *Nature* **2009**, 459 (7245), 379–385. https://doi.org/10.1038/nature08147
12. Weekes, M. P.; Antrobus, R.; Lill, J. R.; Duncan, L. M.; Hör, S.; Lehner, P. J. Comparative Analysis of Techniques to Purify Plasma Membrane *Proteins* **2010**, 21 (3).
13. Haffke, M.; Duckely, M.; Bergsdorf, C.; Jaakola, V.-P.; Shrestha, B. Development of a Biochemical and Biophysical Suite for Integral Membrane Protein Targets: A Review. *Protein Expression and Purification* **2020**, 167, 105545. https://doi.org/10.1016/j.pep.2019.105545
14. White, S. H.; Wimley, W. C. MEMBRANE PROTEIN FOLDING AND STABILITY: Physical Principles. *Annu. Rev. Biophys. Biomol. Struct.* **1999**, 28 (1), 319–365. https://doi.org/10.1146/annurev.biophys.28.1.319
15. Cross, T. A.; Sharma, M.; Yi, M.; Zhou, H.-X. Influence of Solubilizing Environments on Membrane Protein Structures. *Trends in Biochemical Sciences* **2011**, 36 (2), 117–125. https://doi.org/10.1016/j.tibs.2010.07.005
16. Barnaba, C.; Ramamoorthy, A. Picturing the Membrane-Assisted Choreography of Cytochrome P450 with Lipid Nanodiscs. *ChemPhysChem* **2018**, 19 (20), 2603–2613. https://doi.org/10.1002/cphc.201800444
17. Frey, L.; Lakomek, N.-A.; Riek, R.; Bibow, S. Micelles, Bicelles, and Nanodiscs: Comparing the Impact of Membrane Mimetics on Membrane Protein Backbone Dynamics. *Angew. Chem. Int. Ed.* **2017**, 56 (1), 380–383. https://doi.org/10.1002/anie.201608246
18. Oluwole, A.; Shutin, D.; Bolla, J. R. Mass Spectrometry of Intact Membrane Proteins: Shifting towards a more Native-like Context. *Essays in Biochemistry* **2023**, 67, 201-213. https://doi/org/10/1042/EBC20220169
19. Calabrese, A. N.; Radford, S. E. Mass Spectrometry-Enabled Structural Biology of Membrane Proteins. *Methods* **2018**, 147, 187–205. https://doi.org/10.1016/j.ymeth.2018.02.020
20. Konijnenberg, A.; van Dyck, J. F.; Kailing, L. L.; Sobott, F. Extending Native Mass Spectrometry Approaches to Integral Membrane Proteins. *Biological Chemistry* **2015**, 396 (9–10), 991–1002. https://doi.org/10.1515/hsz-2015-0136
21. Konijnenberg, A.; Butterer, A.; Sobott, F. Native Ion Mobility-Mass Spectrometry and Related Methods in Structural

Biology. *Biochimica et Biophysica Acta.* **2013**, 1834, 1239-1256. https://doi.org/10.1016/j.bbapap.2012.11.013

22. Konermann, L.; Ahadi, E.; Rodriguez, A. D.; Vahidi, S. Unraveling the Mechanism of Electrospray Ionization. *Anal Chem*. **2013**. 85, 1, 2-9. https://doi.org/10.1021/ac302789

23. Keener, J. E.; Zhang, G.; Marty, M. T. Native Mass Spectrometry of Membrane Proteins. *Anal. Chem.* **2021**, 93 (1), 583–597. https://doi.org/10.1021/acs.analchem.0c04342

24. Gault, J.; Donlan, J. A. C.; Liko, I.; Hopper, J. T. S.; Gupta, K.; Housden, N. G.; Struwe, W. B.; Marty, M. T.; Mize, T.; Bechara, C.; Zhu, Y.; Wu, B.; Kleanthous, C.; Belov, M.; Damoc, E.; Makarov, A.; Robinson, C. V. High-Resolution Mass Spectrometry of Small Molecules Bound to Membrane Proteins. *Nat Methods* **2016**, 13 (4), 333–336. https://doi.org/10.1038/nmeth.3771

25. Konijnenberg, A.; Yilmaz, D.; Ingólfsson, H. I.; Dimitrova, A.; Marrink, S. J.; Li, Z.; Vénien-Bryan, C.; Sobott, F.; Koçer, A. Global Structural Changes of an Ion Channel during Its Gating Are Followed by Ion Mobility Mass Spectrometry. *Proc. Natl. Acad. Sci. U.S.A.* **2014**, 111 (48), 17170–17175. https://doi.org/10.1073/pnas.1413118111

26. Gupta, K.; Donlan, J. A. C.; Hopper, J. T. S.; Uzdavinys, P.; Landreh, M.; Struwe, W. B.; Drew, D.; Baldwin, A. J.; Stansfeld, P. J.; Robinson, C. V. The Role of Interfacial Lipids in Stabilizing Membrane Protein Oligomers. *Nature* **2017**, 541 (7637), 421–424. https://doi.org/10.1038/nature20820

27. Gupta, K.; Li, J.; Liko, I.; Gault, J.; Bechara, C.; Wu, D.; Hopper, J. T. S.; Giles, K.; Benesch, J. L. P.; Robinson, C. V. Identifying Key Membrane Protein Lipid Interactions Using Mass Spectrometry. *Nat Protoc* **2018**, 13 (5), 1106–1120. https://doi.org/10.1038/nprot.2018.014

28. Landreh, M.; Costeira-Paulo, J.; Gault, J.; Marklund, E. G.; Robinson, C. V. Effects of Detergent Micelles on Lipid Binding to Proteins in Electrospray Ionization Mass Spectrometry. *Anal. Chem.* **2017**, 89 (14), 7425–7430. https://doi.org/10.1021/acs.analchem.7b00922

29. Liko, I.; Degiacomi, M. T.; Lee, S.; Newport, T. D.; Gault, J.; Reading, E.; Hopper, J. T. S.; Housden, N. G.; White, P.; Colledge, M.; Sula, A.; Wallace, B. A.; Kleanthous, C.; Stansfeld, P. J.; Bayley, H.; Benesch, J. L. P.; Allison, T. M.; Robinson, C. V. Lipid Binding Attenuates Channel Closure of the Outer Membrane Protein OmpF. *Proc. Natl. Acad. Sci. U.S.A.* **2018**, 115 (26), 6691–6696. https://doi.org/10.1073/pnas.1721152115

30. Borysik, A. J.; Hewitt, D. J.; Robinson, C. V. Detergent Release Prolongs the Lifetime of Native-like Membrane Protein Conformations in the Gas-Phase. *J. Am. Chem. Soc.* **2013**, 135 (16), 6078–6083. https://doi.org/10.1021/ja401736v

31. Fantin, S. M.; Parson, K. F.; Niu, S.; Liu, J.; Polasky, D. A.; Dixit, S. M.; Ferguson-Miller, S. M.; Ruotolo, B. T. Collision Induced Unfolding Classifies Ligands Bound to the Integral Membrane Translocator Protein. *Anal. Chem.* **2019**, 91 (24), 15469–15476. https://doi.org/10.1021/acs.analchem.9b03208

32. Gault, J.; Liko, I.; Landreh, M.; Shutin, D.; Reddy Bolla J.; Jefferies, D.; Agasid, M.; Yen, HS.; Ladds J.G.W.; Lane D.P.; Khalid, S.; Mullen, C.; Remes P. M.; Huguet, R.; McAlister, G.; Goodwin, M.; Viner, R.; Syka J. E. P.; Robinson C. V. Combining Native and 'Omics' Mass Spectrometry to Identify Endogenous Ligands Bound to Membrane Proteins. *Nature Methods.* **2020**, 17, 505-508. https://doi.org/10.1038/s41592-020-0821-0

33. Watkinson, T. G.; Calabrese, A. N.; Ault, J. R.; Radford, S. E.; Ashcroft, A. E. FPOP-LC-MS/MS Suggests Differences in Interaction Sites of Amphipols and Detergents with Outer Membrane Proteins. *J. Am. Soc. Mass Spectrom.* **2017**, 28 (1), 50–55. https://doi.org/10.1007/s13361-016-1421-1

34. Calabrese, A. N.; Watkinson, T. G.; Henderson, P. J. F.; Radford, S. E.; Ashcroft, A. E. Amphipols Outperform Dodecylmaltoside Micelles in Stabilizing Membrane Protein Structure in the Gas Phase. *Anal. Chem.* **2015**, 87 (2), 1118–1126. https://doi.org/10.1021/ac5037022

35. Watkinson, T. G.; Calabrese, A. N.; Giusti, F.; Zoonens, M.; Radford, S. E.; Ashcroft, A. E. Systematic Analysis of the Use of Amphipathic Polymers for Studies of Outer Membrane Proteins Using Mass Spectrometry. *International Journal of Mass Spectrometry* **2015**, 391, 54–61. https://doi.org/10.1016/j.ijms.2015.06.017

36. Fantin, S. M.; Parson, K. F.; Yadav, P.; Juliano, B.; Li, G. C.; Sanders, C. R.; Ohi, M. D.; Ruotolo, B. T. Ion Mobility–Mass Spectrometry Reveals the Role of Peripheral Myelin Protein Dimers in Peripheral Neuropathy. *Proc. Natl. Acad. Sci. U.S.A.* **2021**, 118 (17), e2015331118. https://doi.org/10.1073/pnas.2015331118

37. Hutchison, J. M.; Shih, K.-C.; Scheidt, H. A.; Fantin, S. M.; Parson, K. F.; Pantelopulos, G. A.; Harrington, H. R.; Mittendorf, K. F.; Qian, S.; Stein, R. A.; Collier, S. E.; Chambers, M. G.; Katsaras, J.; Voehler, M. W.; Ruotolo, B. T.; Huster, D.; McFeeters, R. L.; Straub, J. E.; Nieh, M.-P.; Sanders, C. R. Bicelles Rich in Both Sphingolipids and Cholesterol and Their Use in Studies of Membrane Proteins. *J. Am. Chem. Soc.* **2020**, 142 (29), 12715–12729. https://doi.org/10.1021/jacs.0c04669

38. Keener, J. E.; Zambrano, D. E.; Zhang, G.; Zak, C. K.; Reid, D. J.; Deodhar, B. S.; Pemberton, J. E.; Prell, J. S.; Marty, M. T. Chemical Additives Enable Native Mass Spectrometry Measurement of Membrane Protein Oligomeric State within Intact Nanodiscs. *J. Am. Chem. Soc.* **2019**, 141 (2), 1054–1061. https://doi.org/10.1021/jacs.8b11529

39. Henrich, E.; Peetz, O.; Hein, C.; Laguerre, A.; Hoffmann, B.; Hoffmann, J.; Dötsch, V.; Bernhard, F.; Morgner, N. Analyzing Native Membrane Protein Assembly in Nanodiscs by Combined Non-Covalent Mass Spectrometry and Synthetic Biology. *eLife* **2017**, 6, e20954. https://doi.org/10.7554/eLife.20954

40. Harvey, S. R.; VanAernum, Z. L.; Kostelic, M. M.; Marty, M. T.; Wysocki, V. H. Probing the Structure of Nanodiscs Using Surface-Induced Dissociation Mass Spectrometry. *Chem. Commun.* **2020**, 56 (100), 15651–15654. https://doi.org/10.1039/D0CC05531J

41. Marty, M. T.; Hoi, K. K.; Robinson, C. V. Interfacing Membrane Mimetics with Mass Spectrometry. *Acc. Chem. Res.* **2016**, 49 (11), 2459–2467. https://doi.org/10.1021/acs.accounts.6b00379

42. Marty, M. T. Nanodiscs and Mass Spectrometry: Making Membranes Fly. *International Journal of Mass Spectrometry* **2020**, 458, 116436. https://doi.org/10.1016/j.ijms.2020.116436

43. Hellwig, N.; Peetz, O.; Ahdash, Z.; Tascón, I.; Booth, P. J.; Mikusevic, V.; Diskowski, M.; Politis, A.; Hellmich, Y.; Hänelt, I.; Reading, E.; Morgner, N. Native Mass Spectrometry Goes More Native: Investigation of Membrane Protein Complexes Directly from SMALPs. *Chem. Commun.* **2018**, 54 (97), 13702–13705. https://doi.org/10.1039/C8CC06284F

44. Han, L.; Nguyen, L.; Schmidt, E. N.; Esmaili, M.; Kitova, E. N.; Overduin, M.; Macauley, M. S.; Klassen, J. S. How Choice of Model Membrane Affects Protein–Glycosphingolipid Interactions: Insights from Native Mass Spectrometry. *Anal. Chem.* **2022**, 94 (46), 16042–16049. https://doi.org/10.1021/acs.analchem.2c03067

45. Chorev, D. S.; Robinson, C. V. The Importance of the Membrane for Biophysical Measurements. *Nat Chem Biol* **2020**, 16 (12), 1285–1292. https://doi.org/10.1038/s41589-020-0574-1

46. Chen, S.; Getter, T.; Salom, D. Wu, D.; Quetshlich, D.; Chorev, D. S.; Palczewski, K.; Robinson, C.V. Capturing a Rhodopsin Receptor Signaling Cascade across a Native Membrane. *Nature.* **2022**. 604, 384-390. https://doi.org/10.1038/s41586-022-04547-x

47. Chorev, D. S.; Baker, L. A.; Wu, D.; Beilsten-Edmands, V.; Rouse, S. L.; Zeev-Ben-Mordehai, T.; Jiko, C.; Samsudin, F.; Gerle, C.; Khalid, S.; Stewart, A. G.; Matthews, S. J.; Grünewald, K.; Robinson, C. V. Protein Assemblies Ejected Directly from Native Membranes Yield Complexes for Mass Spectrometry. *Science* **2018**, 362 (6416), 829–834. https://doi.org/10.1126/science.aau0976

48. Panda, A.; Giska, F.; Duncan, A. L.; Welch, A. J.; Brown, C.; McAllister, R.; Hariharan, P.; Goder, J. N. D.; Coleman, J.; Ramakrishnan, S.; Pincet, F.; Guan, L.; Krishnakumar, S.; Rothman, J. E.; Gupta, K. Direct Determination of Oligomeric Organization of Integral Membrane Proteins and Lipids from Intact Customizable Bilayer.

Nat Methods **2023**, 20 (6), 891–897. https://doi.org/10.1038/s41592-023-01864-5

49. Panda, A.; Brown, C.; Gupta, K. Studying Membrane Protein-Lipid Specificity through Direct Native Mass Spectrometric Analysis from Tunable Proteoliposomes. *J. Am. Soc. Mass Spectrom.* **2023**. 34 (9), 1917-1927. https://doi.org/10.1021/jasms.3c00110

50. Olinares, P. D. B.; Kang, J. Y.; Llewellyn, E.; Chiu, C.; Chen, J.; Malone, B.; Saecker, R. M.; Campbell, E. A.; Darst, S. A.; Chait, B. T. Native Mass Spectrometry-Based Screening for Optimal Sample Preparation in Single-Particle Cryo-EM. *Structure* **2021**, 29 (2), 186-195.e6. https://doi.org/10.1016/j.str.2020.11.001

51. Konijnenberg, A.; Bannwarth, L.; Yilmaz, D.; Koçer, A.; Venien-Bryan, C.; Sobott, F. Top-down Mass Spectrometry of Intact Membrane Protein Complexes Reveals Oligomeric State and Sequence Information in a Single Experiment. *Protein Science.* **2015**. 24 (8), 1292-1300. https://doi.org/10.1002/pro.2703

52. Marty, M. T.; Hoi, K. K.; Gault, J.; Robinson, C. V. Probing the Lipid Annular Belt by Gas-Phase Dissociation of Membrane Proteins in Nanodiscs. *Angew. Chem. Int. Ed.* **2016**, 55 (2), 550–554. https://doi.org/10.1002/anie.201508289

53. Keener, J. E.; Jayasekera, H. S.; Marty, M. T. Investigating the Lipid Selectivity of Membrane Proteins in Heterogenous Nanodiscs. *Anal Chem.* **2022**. 94 (23), 8497-8505. https://doi.org/10.1021/acs.analchem.2c01488

54. Liu, Y.; Cong, X.; Liu, W.; Laganowsky, A. Characterization of Membrane Protein–Lipid Interactions by Mass Spectrometry Ion Mobility Mass Spectrometry. *J. Am. Soc. Mass Spectrom.* **2017**, 28 (4), 579–586. https://doi.org/10.1007/s13361-016-1555-1

55. Wang, S. C.; Politis, A.; Di Bartolo, N.; Bavro, V. N.; Tucker, S. J.; Booth, P. J.; Barrera, N. P.; Robinson, C. V. Ion Mobility Mass Spectrometry of Two Tetrameric Membrane Protein Complexes Reveals Compact Structures and Differences in Stability and Packing. *J. Am. Chem. Soc.* **2010**, 132 (44), 15468–15470. https://doi.org/10.1021/ja104312e

56. Harvey, S. R.; O'Neale, C.; Schey, K. L.; Wysocki, V. H. Native Mass Spectrometry and Surface Induced Dissociation Provide Insight into the Post-Translational Modifications of Tetrameric AQP0 Isolated from Bovine Eye Lens. *Anal. Chem.* **2022**, 94 (3), 1515–1519. https://doi.org/10.1021/acs.analchem.1c04322

57. Ruotolo, B. T.; Benesch, J. L. P.; Sandercock, A. M.; Hyung, S.-J.; Robinson, C. V. Ion Mobility–Mass Spectrometry Analysis of Large Protein Complexes. *Nat Protoc* **2008**, 3 (7), 1139–1152. https://doi.org/10.1038/nprot.2008.78

58. Polasky, D. A.; Dixit, S. M.; Vallejo, D. D.; Kulju, K. D.; Ruotolo, B. T. An Algorithm for Building Multi-State Classifiers Based on Collision-Induced Unfolding Data. *Anal. Chem.* **2019**, 91 (16), 10407–10412. https://doi.org/10.1021/acs.analchem.9b02650

59. Barrera, N. P.; Isaacson, S. C.; Zhou, M.; Bavro, V. N.; Welch, A.; Schaedler, T. A.; Seeger, M. A.; Miguel, R. N.; Korkhov, V. M.; van Veen, H. W.; Venter, H.; Walmsley, A. R.; Tate, C. G.; Robinson, C. V. Mass Spectrometry of Membrane Transporters Reveals Subunit Stoichiometry and Interactions. *Nat Methods* **2009**, 6 (8), 585–587. https://doi.org/10.1038/nmeth.1347

60. Landreh, M.; Liko, I.; Uzdavinys, P.; Coincon, M.; Hopper, J. T. S.; Drew, D.; Robinson, C. V. Controlling Release, Unfolding and Dissociation of Membrane Protein Complexes in the Gas Phase through Collisional Cooling. *Chem. Commun.* **2015**, 51 (85), 15582–15584. https://doi.org/10.1039/C5CC07045G

61. Laganowsky, A.; Reading, E.; Allison, T. M.; Ulmschneider, M. B.; Degiacomi, M. T.; Baldwin, A. J.; Robinson, C. V. Membrane Proteins Bind Lipids Selectively to Modulate Their Structure and Function. *Nature* **2014**, 510 (7503), 172–175. https://doi.org/10.1038/nature13419

62. Allison, T. M.; Reading, E.; Liko, I.; Baldwin, A. J.; Laganowsky, A.; Robinson, C. V. Quantifying the Stabilizing Effects of Protein–Ligand Interactions in the Gas Phase. *Nat Commun* **2015**, 6 (1), 8551. https://doi.org/10.1038/ncomms9551

63. Wade, J. H.; Jones, J. D.; Lenov, I. L.; Riordan, C. M.; Sligar, S. G.; Bailey, R. C. Microfluidic Platform for Efficient Nanodisc Assembly, Membrane Protein Incorporation, and Purification. *Lab Chip* **2017**, 17 (17), 2951–2959. https://doi.org/10.1039/C7LC00601B

64. Hosea, N. A.; Miller, G. P.; Guengerich, F. P. Elucidation of Distinct Ligand Binding Sites for Cytochrome P450 3A4. *Biochemistry* **2000**, 39 (20), 5929–5939. https://doi.org/10.1021/bi992765t

65. Schlebach, J. P.; Peng, D.; Kroncke, B. M.; Mittendorf, K. F.; Narayan, M.; Carter, B. D.; Sanders, C. R. Reversible Folding of Human Peripheral Myelin Protein 22, a Tetraspan Membrane Protein. *Biochemistry* **2013**, 52 (19), 3229–3241. https://doi.org/10.1021/bi301635f

66. Kermani, A. A.; Macdonald, C. B.; Gundepudi, R.; Stockbridge, R. B. Guanidinium Export Is the Primal Function of SMR Family Transporters. *Proc. Natl. Acad. Sci. U.S.A.* **2018**, 115 (12), 3060–3065. https://doi.org/10.1073/pnas.1719187115

67. Laganowsky, A.; Reading, E.; Hopper, J. T. S.; Robinson, C. V. Mass Spectrometry of Intact Membrane Protein Complexes. *Nat Protoc* **2013**, 8 (4), 639–651. https://doi.org/10.1038/nprot.2013.024

68. Sligar, S. G.; Denisov, I. G. Nanodiscs: A Toolkit for Membrane Protein Science. *Protein Science* **2021**, 30 (2), 297–315. https://doi.org/10.1002/pro.3994

69. Denisov, I. G.; Sligar, S. G. Nanodiscs in Membrane Biochemistry and Biophysics. *Chem. Rev.* **2017**, 117 (6), 4669–4713. https://doi.org/10.1021/acs.chemrev.6b00690

70. Haynes, S. E.; Polasky, D. A.; Dixit, S. M.; Majmudar, J. D.; Neeson, K.; Ruotolo, B. T.; Martin, B. R. Variable-Velocity Traveling-Wave Ion Mobility Separation Enhancing Peak Capacity for Data-Independent Acquisition Proteomics. *Anal. Chem.* **2017**, 89 (11), 5669–5672. https://doi.org/10.1021/acs.analchem.7b00112

71. Polasky, D. A.; Dixit, S. M.; Vallejo, D. D.; Kulju, K. D.; Ruotolo, B. T. An Algorithm for Building Multi-State Classifiers Based on Collision-Induced Unfolding Data. *Anal. Chem.* **2019**, 91 (16), 10407–10412. https://doi.org/10.1021/acs.analchem.9b02650

72. Richardson, K.; Langridge, D.; Dixit, S. M.; Ruotolo, B. T. An Improved Calibration Approach for Traveling Wave Ion Mobility Spectrometry: Robust, High-Precision Collision Cross Sections. *Anal. Chem.* **2021**, 93 (7), 3542–3550. https://doi.org/10.1021/acs.analchem.0c04948

73. Kermani, A. A.; Macdonald, C. B.; Burata, O. E.; Ben Koff, B.; Koide, A.; Denbaum, E.; Koide, S.; Stockbridge, R. B. The Structural Basis of Promiscuity in Small Multidrug Resistance Transporters. *Nat Commun* **2020**, 11 (1), 6064. https://doi.org/10.1038/s41467-020-19820-8

74. Mittendorf, K. F.; Kroncke, B. M.; Meiler, J.; Sanders, C. R. The Homology Model of PMP22 Suggests Mutations Resulting in Peripheral Neuropathy Disrupt Transmembrane Helix Packing. *Biochemistry* **2014**, 53 (39), 6139–6141. https://doi.org/10.1021/bi500809t

75. Parson, K. F. Development of Ion Mobility-Mass Spectrometry Methods for Membrane Proteins Incorporated into Nanodiscs. Ph.D. Dissertation, University of Michigan: Ann Arbor, MI, **2022**. https://dx.doi.org/10.7302/6268

76. Marklund, E. G.; Degiacomi, M. T.; Robinson, C. V.; Baldwin, A. J.; Benesch, J. L. P. Collision Cross Sections for Structural Proteomics. *Structure* **2015**, 23 (4), 791–799. https://doi.org/10.1016/j.str.2015.02.010

77. Dutta, S.; Morrison, E. A.; Henzler-Wildman, K. A. EmrE Dimerization Depends on Membrane Environment. *Biochimica et Biophysica Acta (BBA) - Biomembranes* **2014**, 1838 (7), 1817–1822. https://doi.org/10.1016/j.bbamem.2014.03.013

78. Park, S. J.; Kern, N.; Brown, T.; Lee, J.; Im, W. CHARMM-GUI PDB Manipulator: Various PDB Structural Modifications for Biomolecular Modeling and Simulation. *J Mol Biol.* **2023**, 435, 167996. https://10.1016/j.jmb.2023.167995

79. Sahin, C.; Reid, D. J.; Marty, M. T.; Landreh, M. Scratching the Surface: Native Mass Spectrometry of Peripheral Membrane Protein Complexes. *Biochemical Society Transactions* **2020**, 48 (2), 547–558. https://doi.org/10.1042/BST20190787

80. Allen, K. N.; Entova, S.; Ray, L. C.; Imperiali, B. Monotopic Membrane Proteins Join the Fold. *Trends in Biochemical Sciences* **2019**, 44 (1), 7–20. https://doi.org/10.1016/j.tibs.2018.09.013

81. Denisov, I. G.; Sligar, S. G. Cytochromes P450 in Nanodiscs. *Biochimica et Biophysica Acta (BBA) - Proteins and Proteomics* **2011**, 1814 (1), 223–229. https://doi.org/10.1016/j.bbapap.2010.05.017

82. Shah, M. B.; Jang, H.-H.; Wilderman, P. R.; Lee, D.; Li, S.; Zhang, Q.; Stout, C. D.; Halpert, J. R. Effect of Detergent Binding on Cytochrome P450 2B4 Structure as Analyzed by X-Ray Crystallography and Deuterium-Exchange Mass Spectrometry. *Biophysical Chemistry* **2016**, 216, 1–8. https://doi.org/10.1016/j.bpc.2016.05.007

83. Lössl, P.; Snijder, J.; Heck, A. J. R. Boundaries of Mass Resolution in Native Mass Spectrometry. *J. Am. Soc. Mass Spectrom.* **2014**, 25 (6), 906–917. https://doi.org/10.1007/s13361-014-0874-3

84. Grinkova, Y. V.; Denisov, I. G.; Sligar, S. G. Functional Reconstitution of Monomeric CYP3A4 with Multiple Cytochrome P450 Reductase Molecules in Nanodiscs. *Biochemical and Biophysical Research Communications* **2010**, 398 (2), 194–198. https://doi.org/10.1016/j.bbrc.2010.06.058

85. Juliano, B. R.; Keating, J. W.; Ruotolo, B.T. Infrared Photoactivation Enables Improved Native Top-Down Mass Spectrometry of Transmembrane Proteins. *Anal Chem.* **2023**, 95 (35), 13361-13367. https://doi.org/10.1021/acs.analchem.3c02788

86. Hellwig, N.; Martin, J.; Morgner, N. LILBID-MS: using Lasers to Shed Light on Biomolecular Architectures. *Biochem Soc Trans.* **2022**, 50 (3), 1057-1067. https://doi.org/10.1042/BST20190881

87. Zhu, Y.; Peng, B. J.; Kumar, S.; Stover, L.; Chang, J. Y.; Lyu, J.; Schrecke, S.; Azizov, D.; Russell, D. H.; Fang, L.; Laganowsky, A. Polyamine Detergents Tailored for Native Mass Spectrometry Studies of Membrane Proteins. *Nature Communications*. **2023**, 14, 5676. https://doi.org/10.1038/s41467-023-41429-w

88. Behnke, J. S.; Urner, L. H. Emergence of Mass Spectrometry Detergents for Membrane Proteomics. *Anal Bioanal Chem.* **2023**, 415, 3897-3909. https://doi.org/10.1007/s00216-023-04584-z

89. Alford, R. F.; Leaver-Fay, A.; Jeliazkov, J. R,; O'Meara, M. J.; DiMaio, F. P.; Park, H.; Shapovalov, M. V.; Renfrew, P. D.; Mulligan, V. K.; Kappel, K.; Labonte, J. W.; Pacella, M. S.; Bonneau, R.; Bradley, P.; Dunbrack, R. L. Jr.; Das, R.; Baker, D,; Kuhlman, B.; Kortemme, T.; Gray, J. J. The Rosetta All-Atom Energy Function for Macromolecular Modeling and Design. *J Chem Theory Comput.* **2017**, 13 (6), 3031-3048. https://doi.org/10.1007/s00216-023-04584-z

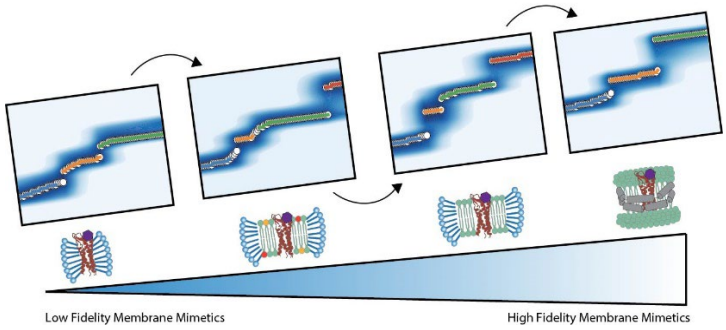

For Table of Contents Use Only